Drug Development and Industrial Pharmacy, 2010; 36(10): 1235–1244

informa
healthcare

ORIGINAL ARTICLE

Synthesis, self-assembly, and characterization of PEG-coated iron oxide nanoparticles as potential MRI contrast agent

Chen Yue-Jian[1,2], Tao juan[1,2], Xiong Fei[2], Zhu Jia-Bi[1], Gu Ning[2], Zhang Yi-Hua[3], Ding Ye[3] and Ge Liang[1]

[1]Pharmaceutical Research Institute, China Pharmaceutical University, Nanjing, PR China, [2]State Key Laboratory of Bioelectronics, Jiangsu Laboratory for Biomaterials and Devices, School of Biological Science and Medical Engineering, Southeast University, Nanjing, PR China and [3]Centre of Drug Research, China Pharmaceutical University, Nanjing, PR China

Abstract

Aim: Investigated the self-assembly and characterization of novel antifouling polyethylene glycol (PEG)-coated iron oxide nanoparticles as nanoprobes for magnetic resonance imaging (MRI) contrast agent. *Method*: Monodisperse oleic acid-coated superparamagnetic iron oxide cores are synthesized by thermal decomposition of iron oleate. The self-assembly behavior between iron oxide cores and PEG-lipid conjugates in water and their characteristics are confirmed by transmission electron microscope, X-ray diffraction, thermogravimetric analysis, Fourier transform infrared spectroscopy, and vibrating sample magnetometer. *Result*: Dynamic light scattering shows superparamagnetic iron oxide nanoparticles coated with PEG are stable in water for pH of 3–10 and ionic strengths up to 0.3 M NaCl, and are protein resistant in physiological conditions. Additionally, in vitro MRI study demonstrates the efficient magnetic resonance imaging contrast characteristics of the iron oxide nanoparticles. *Conclusion*: The result indicates that the novel antifouling PEG-coated superparamagnetic iron oxide nanoparticles could potentially be used in a wide range of applications such as biotechnology, MRI, and magnetic fluid hyperthermia.

Key words: *CMC; magnetic nanoparticles; monodisperse; MRI; self-assembly; superparamagnetic iron oxide nanoparticles; thermal decomposition*

Introduction

Magnetic nanoparticles (MNPs) with appropriate surface chemical properties have been widely used for various biomedical applications such as magnetic resonance imaging (MRI) contrast enhancement[1,2], tissue repair[3], hyperthermia[4], targeted drug delivery[5], cell separation[6], and so on. Among MNPs, iron oxide nanoparticles are particularly attractive for above applications because of their size-dependent superparamagnetism, low toxicity, and biocompatibility with cells and tissue[7]. Therefore, iron oxide nanoparticles may potentially provide higher-contrast enhancement in MRI than conventional paramagnetic Gd-based contrast agents[8] because of their superparamagnetic property. Moreover, MNPs with suitable particle size can specifically accumulate in tumor sites by enhanced permeability and retention (EPR) effect as a result of the presence of leaky vasculatures around tumors[9].

To take advantage of their high-quality and uniform imaging property in MRI and specific tumor targeting, it is desirable to obtain iron oxide nanoparticles with controlled-shape, controlled-size, and narrow-size distribution. Very recently, several groups have reported that such high-quality iron oxide nanoparticles could be synthesized by thermal decomposition of different types of iron precursors such as iron acetylacetonate[10], iron pentacarbonyl[11], and iron oleate[12,13]. Nanoparticles

Address for correspondence: Zhu Jia-Bi, Pharmaceutical Research Institute, China Pharmaceutical University, 24 Tongjiaxiang, Nanjing 210009, PR China. Tel: +86 25 83271316. E-mail: Zhu_Jiabi@163.com

(Received 29 Oct 2009; accepted 16 Feb 2010)

ISSN 0363-9045 print/ISSN 1520-5762 online © Informa UK, Ltd.
DOI: 10.3109/03639041003710151

synthesized by these methods are monodisperse and single crystalline with high-magnetic moment compared with those prepared from co-precipitation of Fe^{2+} and Fe^{3+} salt mixture in base aqueous solution[14]. However, the direct products of the above-mentioned thermal decomposition approaches are organic-soluble, which to some extent limits their applications in biological fields. Therefore, it is essential to engineer the surface of iron oxide nanoparticles with hydrophilic molecules to minimize aggregation of the particles and nonspecific uptake by mononuclear phagocyte system in physiological conditions for long periods[15,16].

To inhibit the plasma adsorption and escape from the uptake by mononuclear phagocyte system, several synthetic and natural polymers have been employed to modify the surface of the particles to enhance their function in vivo. These polymers include starch[17], dextran[18], dendrimers[19], polyethylene glycol (PEG)[20], and polyethylene oxide[21], all of which are known to be biocompatible and surface modification results in a long blood circulation time. Several attempts have been made to modify the iron oxide cores with polymer while retaining their inherent strong magnetic and imaging properties. In the commonly used approach, the polymer is covalently linked to the surface of iron oxide cores. This approach requires developing complex conjugation chemistry and is impractical to synthesize in large amounts on an industrial scale. In another approach, iron oxide cores are dispersed in polymers (e.g., poly-DL-lactide-*co*-glycolide[22], polylactide[23], dendrimers[19]) that are typically used in developing other nanocarriers for drug delivery application. However, this approach usually leads to the formation of large-sized microparticles with limited encapsulation of MNPs resulting in significant loss in magnetization (~40–50%) of the iron oxide cores[24], which could adversely influence its imaging property. Therefore, the use of MNPs for MRI must address issues such as stability in physiology environment in terms of evasion from agglomeration and macrophage uptake, retention of magnetic properties after modification with polymers, and high contrast enhancement.

We had recently developed a formulation of MNPs coated with PEGylated bilayers, in which the iron oxide cores were first coated with oleic acid (OA, inner layer) and then OA-coated particles were stabilized with PEG-lipid conjugates (DO-PEG, outer layer) to form a water dispersible system. The PEG-lipid conjugates were synthesized using a simple and inexpensive method, which were physically interdigitated with the OA layer through self-assembly method. In this study we examined the feasibility of this polymer conjugates as an antifouling coating material for MNPs. Especially, we analyzed (1) the synthesis, self-assembly, and superparamagnetic characteristics of PEG-coated MNPs, (2) the stability of MNPs at physiological conditions, (3) the efficacy as MRI contrast agent using 7.0 T MRI scanner.

Materials and methods

Materials

Reagents and solvents were commercially available and used as supplied without further purification unless otherwise stated. L-Lysine methyl ester was synthesized using literature methodology[25]. Oleic acid chloride had previously been reported in our previous paper[26] and data were therefore not provided here. All solutions of $NaHCO_3$ were saturated aqueous solutions. All solutions of $NaHSO_4$ were aqueous solutions (160 g/dm^3). Methyl-poly(ethylene glycol) with Mn 2000 g/mol were precipitated from tetrahydrofuran solution into ether. CH_2Cl_2 was refluxed over P_2O_5 and then distilled. 1-Ethyl-3-(3-dimethylaminopropyl)carbodiimide hydrochloride and 4-dimethylaminopyridine were obtained from Shanghai Medpep Co., Ltd., Shanghai, China.

Characterization

All the compounds synthesized were purified by column chromatography on silica gel 60 (200–300 mesh) and thin-layer chromatography on silica gel 60 F_{254} plates (250 μm; Qingdao Ocean Chemical Company, Qingdao, China). Infrared spectra were recorded on KBr pellets by Nicolet Nexus 870 Fourier transform infrared spectroscopy (FT-IR) spectrometer. Nuclear magnetic resonance (NMR) spectra were obtained on a Bruker AV-500 NMR Spectrometer operating at 500 MHz. The pyrene fluorescence spectra were recorded on a Perkin-Elmer LS-50B spectrofluorometer. Powder X-ray diffraction (XRD) patterns were acquired from dried nanoparticle samples with a ARL X'TRA X-ray diffractometer using Cu K_α radiation ($\lambda = 1.541$Å) at 40 kV and 40 mA. Thermogravimetric analysis (TGA) was performed for powder samples (~5 mg) with a heating rate of 20°C/min using a Perkin-Elmer TGA7 Thermogravimetric Analyzer in synthetic N_2 atmosphere up to 700°C. Magnetic measurements were carried out with a Lakeshore 7470 vibrating sample magnetometer (VSM) at room temperature.

General synthetic procedures of DO-PEG conjugates

The strategy of synthesis described in Figure 1 consisted of three main parts: (1) condensation of long-chain (oleoyl) fatty acids to the lysine which prepare the N^{α},N^{ε}-dioxyl lysine (hydrophobic part); (2) preparation of hydrophilic methyl-polyoxyethylene amine (hydrophilic part); and (3) condensation of the hydrophobic modified lysine with the hydrophilic moiety to obtain

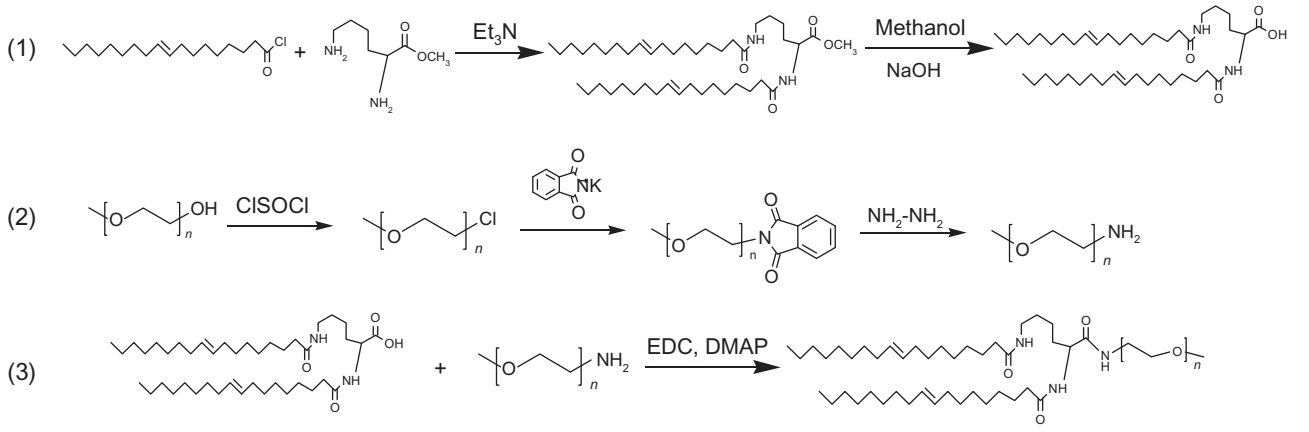

Figure 1. Schematic representation of the synthesis of the PEG-lipid conjugates.

the final nonionic amphiphilic compounds from lysine (coupling part).

L-Lysine methyl ester dihydrochloride (6.4 mmol) was suspended in dichloromethane (DCM) (60 mL). Et_3N (32 mmol) and oleic acid chloride (12.8 mmol) were added to this suspension and stirred for 24 hours under nitrogen. The precipitate was removed by filtration and washed with DCM. The filtrate was washed with $NaHCO_3$, $NaHSO_4$, $NaHCO_3$, water, and then dried over $MgSO_4$. The volatiles were removed by rotary evaporation, and the crude product was purified by silica column chromatography (DCM–MeOH, 98:2).

Di-oleoyl-L-lysine methyl ester (2.6 mmol) was dispersed in the mixture of MeOH (30 mL) and aqueous NaOH (1 M, 7.8 mmol) and stirred for 1 day. The volatiles were removed by rotary evaporation and acidified to pH 3. The solid was collected by filtration, washed with water, and finally dried under high vacuum for 48 hours.

Amino-mPEG (mPEG-NH_2) was synthesized by a three-step reaction starting from mPEG according to the previously described method[27]. Briefly, $mPEG_{2000}$ (5 mmol) was converted to chloro-mPEG (mPEG-Cl) by reflux with thionyl chloride (20 mmol). Subsequently, phtalimido-mPEG (mPEG-PT) was obtained by nucleophilic displacement of chlorine group of mPEG-Cl with phthalimide (10 mmol) at 100°C for 4 hours. Finally, hydrazinolysis of the phthalimide end group was performed to produce mPEG-NH_2 by reflux with hydrazine hydrate (20 mmol) for 12 hours. The product was purified by precipitation from ether.

Di-oleoyl-L-lysine (0.2 mmol) and 1-Ethyl-3-(3-dimethylaminopropyl)carbodiimide (EDC) (0.2 mmol) were dissolved in 50 mL DCM and stirred for 30 minutes. Amino-mPEG (0.2 mmol) and 4-Dimethylaminopyridine (DMAP) (0.2 mmol) were added to the mixture and stirred for 6 hours. The product precipitated from ether was further purified by column chromatography (silica gel, chloroform/methanol, 10/1, v/v).

Determination of critical micelle concentration of DO-PEG conjugates

The critical micelle concentration (CMC) of DO-PEG was determined by fluorescence probe technique using pyrene as a probe. Fluorescence spectra were obtained with a fluorescence spectrometer (LS-50B, Perkin-Elmer). Aliquots of pyrene solution (2×10^{-5} M in acetone, 1 mL) were added to a series of 20-mL vials, and acetone was allowed to evaporate at room temperature. Ten milliliters of polymer aqueous solutions with different concentrations (C_p = 0.0001–0.2 mg/mL) was added to these vials. The solutions were sonicated for 2 hours at 65°C and then kept at room temperature for 24 hours to allow the solubilization equilibrium of pyrene. The samples were then analyzed by fluorescent spectroscopy, with an emission wavelength of 390 nm. The CMC was determined by taking a midpoint of the DO-PEG conjugates concentration at which the relative excitation fluorescence intensity ratio measured at 338–333 nm was varied rapidly.

Synthesis of monodisperse MNPs coated with oleic acid

Known method was followed to synthesize OA-coated monodisperse Fe_3O_4 nanoparticles[28]. Monodisperse Fe_3O_4 nanoparticles were synthesized in two steps: first, to prepare an iron oleate precursor and second, to decompose the precursor. In a typical experiment, 1.08 g of $FeCl_3 \cdot 6H_2O$ and 3.65 g of sodium oleate were dissolved in a mixture solvent composed of 8 mL ethanol, 6 mL distilled water, and 14 mL hexane. The solution was heated to 70°C and stirred at this temperature for 4 hours. When the reaction was completed, the upper red-brownish organic layer containing the iron oleate complex was separated and washed three times with 3 mL of distilled water in a separatory funnel. After washing, hexane was evaporated off, washed twice with

ethanol, and then dried under vacuum overnight to remove all solvents. The obtained waxy iron oleate was dissolved in 1-octadecanol at 70°C and reserved as a stable stock solution at room temperature.

One milliliter of the above stock solution (0.39 mol/mL) was mixed with 4 mL 1-octadecanol and 0.5 mL oleic acid. The mixture was heated to 320°C with a constant heating rate of 3.3°C/min under a nitrogen atmosphere, and then kept at that temperature for 30 minutes. The resulting solution was cooled and precipitated by addition of excess ethanol and centrifugation. Then, the precipitate containing OA-coated Fe_3O_4 nanoparticles was washed four to five times with ethanol.

Surface modification of OA-coated magnetic nanoparticles with DO-PEG

Water-stable PEG-coated magnetic nanoparticles were prepared via the self-assembly method. Briefly, 80 mg of DO-PEG and OA-coated Fe_3O_4 nanoparticles (10 mg) were dissolved in tetrahydrofuran (THF) (2 mL). The above solution was slowly added into 5 mL of deionized water under sonication using an ultrasonic generator (KQ116; Ultrasonic Instrument Co., Ltd., Kunshan, China) and then dialyzed against deionized water for 2 days (Mw cut-off: 14,000 Da) to allow the formation of MNPs and to remove organic solvent. Afterward, the nanoparticle solution was removed from the dialysis bag, filtered through a 0.22-μm membrane to remove large aggregates and was directly freeze-dried without cryoprotectant.

Particle size distribution and transmission electron microscope measurements

The particle sizes of MNPs were measured with a photon correlation spectrometer light scattering apparatus zeta potential/particle sizer 3000HS (Malvern Instruments, Worcestershire, UK) and analyzed by the Zetasizer 3000H (MALVERN software).

Transmission electron microscope (TEM) observation of OA-coated magnetic nanoparticles (MNPs-1) in hexane and PEG-coated magnetic nanoparticles (MNPs-2) in double-distilled water were photographed with an H-7650 TEM (Hitachi, Japan) at an acceleration voltage of 100 kV. The above solutions were dropped onto a carbon-coated copper grid, forming a thin liquid film. The films on the grid were negatively stained by adding immediately a drop of 2 wt.% phosphotungstic acid and then air dried.

Measurement of MRI characteristics of MNPs

Suspensions of MNPs in the concentration range of 0–0.8 μg/mL of iron were prepared in 2% agarose solution and scanned under a Bruker Biospec 7.0 T MRI scanner (Bruker Biospin Corporation, Billerica, MA, USA) at room temperature. T_2-weighted images were acquired using the following parameters: repetition time/echo time (TR/TE), 2500/10 ms; display field of view (DFOV), 4.5 × 4.5 mm; matrix, 256 × 256; slice thickness, 1 mm. After acquiring the images, the magnitudes of image intensities T_2 were measured within manually drawn regions of interest for each of the samples. Relaxation rates R_2 ($R_2 = 1/T_2$) were calculated with the T_2 of different iron concentration. T_2 relaxivity was then calculated as slope from a plot R_2 versus iron concentration in agarose solution.

Results and discussion

Synthesis and characterization of DO-PEG conjugates

The main aim of our study was to obtain functionalized PEG-lipid conjugates conferring steric stabilization to MNPs, which was easier to be obtained on an industrial scale than PEG-PE[29]. The surface of the iron oxide core was capped with a monolayer of oleic acid, which minimized the size distribution and aggregation of the magnetic cores in the process of thermal decomposition. PEG-lipid conjugates containing di-oleoyl chains as hydrophobic part seemed quite appropriate for self-assembly of water-dispersed MNPs.

OA_2-Ly was prepared according to the method of Hardy et al.[30] except the long-chain fatty acid. Oleoyl chains were connected to the amino groups of lysine methyl ester using a simple synthetic method based on acid chloride chemistry. Deprotection of the methyl ester was achieved by saponification with aqueous sodium hydroxide in methanol to obtain the N^{α},N^{ε}-dioxyl lysine (hydrophobic part). In the ^{1}H NMR spectra (Figure 3d), the two amide protons (NH) were observed at 6.71 and 5.82 ppm. Furthermore, it was observed that the band at 1733 and 1649 cm^{-1} (Figure 2e) were the characteristic carbonyl strengthening vibration of acid and amide, respectively. These results confirmed the formation of amide by reaction between the amino groups in lysine and oleic acid chloride.

mPEG-NH_2 was prepared by converting terminal hydroxyl group of mPEG to more reactive primary amino group. It was synthesized by a three-step reaction starting from mPEG-OH according to the reported procedure[27]. It could be seen that the FT-IR spectra of all intermediate products and mPEG-NH_2 were different from mPEG as shown in Figure 2. For mPEG-Cl (Figure 2b), two characteristic peaks could be observed at 1111 cm^{-1} (–CH_2–O–CH_2–) and 664 cm^{-1} (C–Cl), and the peak at 3300–3500 cm^{-1} for OH of mPEG disappeared. Then for mPEG-PT (Figure 2c), two characteristic peaks appeared at 1713 and 843 cm^{-1} because of the presence

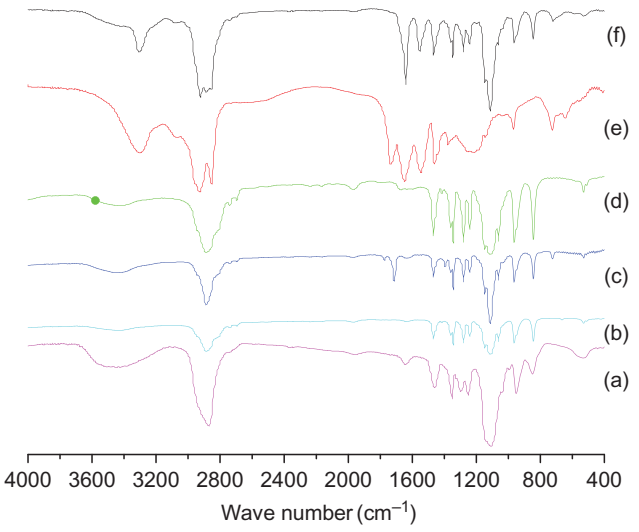

Figure 2. FTIR spectra of (a) mPEG, (b) mPEG-Cl, (c) mPEG-PT, (d) mPEG-NH2, (e) OA_2-Ly, and (f) DO-PEG.

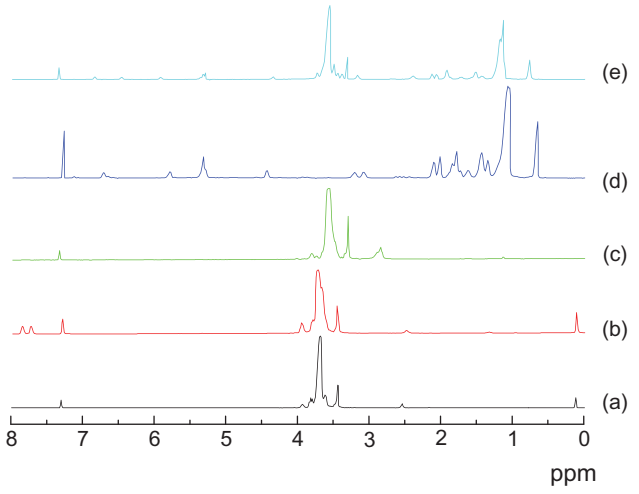

Figure 3. ^{1}H NMR spectra of (a) mPEG-Cl, (b) mPEG-PT, (c) mPEG-NH_2, (d) OA_2-Ly, and (e) DO-PEG.

of phthalimide while the peak at 664 cm^{-1} (C–Cl) disappeared. Subsequently for the mPEG-NH_2 (Figure 2d), the characteristic peak appeared at 3300–3600 cm^{-1} which was assigned to terminal amino groups, while the peak at 1713 cm^{-1} disappeared. In the ^{1}H NMR of mPEG-PT (Figure 3b), the two- and three-position protons in phthalimide were found at 7.84 and 7.72 ppm, respectively. The other peaks of all intermediate products were the same as mPEG-NH_2 (Figure 3c), which implied that the basic structure of PEG did not change except for the conversion of terminal groups.

In the last step, DO-PEG conjugates were prepared using the corresponding mPEG-NH_2 as reagent and 4-dimethylaminopyridine as catalyst. EDC was added as a condensation agent by activating carboxyl acid of OA_2-Ly to form an *O*-acylisourea derivative. The coupling reaction was fast and was easily monitored by thin-layer chromatography. The purification was carried out by recrystallization from diethyl ether and the product was chromatographed with dichloromethane/methanol as eluent. The ^{1}H NMR spectra (Figure 3e) showed the existence of three amide protons (NH). The amide proton joined the mPEG chain that appeared at 6.45 ppm. The signals at 4.38 ppm were attributed to the methine proton of lysine group. Signals at 3.54–3.65 ppm were assigned to the repeating units in PEG. The methylene groups of oleic acid were found at 1.19–1.36 ppm. In addition, the absence of the carbonyl group corresponding to carboxyl acid (FT-IR, ν = 1733 cm^{-1}) (Figure 2f) indicated that the starting material, N^{α},N^{ε}-dioxyl lysine was not present. All these results indicated that the condensation had definitely occurred.

Critical micelle concentration of DO-PEG

CMC was estimated to prove the potential of micelle formation of DO-PEG conjugates in an aqueous environment. The CMC of conjugates was determined by employing pyrene as a fluorescence probe[31]. Pyrene partitioned into the hydrophobic core, and the ratio of fluorescence emission intensities (I_{338}/I_{333}) was varied dramatically because of the formation of micelles. I_{338} and I_{333} represented the value of the band in the pyrene excitation spectra and the value of pyrene entirely in the hydrophobic core of polymeric micelle, respectively. Plots of I_{338}/I_{333} versus log *C* of DO-PEG conjugates were shown in Figure 4. A flat region existed at the low concentration extreme and a sigmoidal region was evident in the crossover region. This result indicated that a midpoint of the conjugates concentration could be evaluated to determine the CMC values of DO-PEG. As shown in Figure 4, the estimated CMC value for the

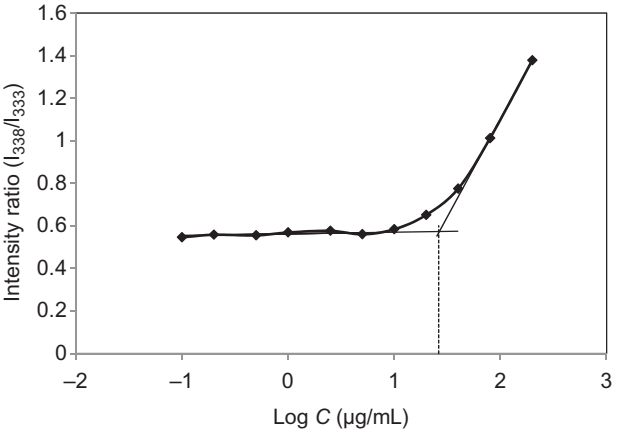

Figure 4. Determination of CMC value of DO-PEG_{2000} using pyrene as fluorescence probe.

conjugates was about 37.3 ± 0.9 μg/mL. Compared with many low-molecular-weight surfactants, such a low CMC meant high thermodynamic stability and potential use of intravenous injection.

Synthesis and self-assembly of PEG-coated magnetic nanoparticles

Hydrophobic OA-coated monodisperse Fe_3O_4 nanoparticles (MNPs-1) were synthesized by thermal decomposition of iron oleate in the presence of oleic acid. The first advantage of this procedure based on iron oleate decomposition was that iron oleate was inexpensive and nontoxic. The second one was that iron oxide NPs could be prepared in a wide range of sizes (from 6 to 30 nm) merely by varying the reaction conditions. The TEM image (Figure 5a) showed that MNPs-1 was monodisperse. The average core particle size and standard deviation obtained from over 300 particles in SEM image using analytic software (Image-Pro Plus 6.0) was about 10.4 ± 0.8 nm.

To transfer hydrophobic OA-coated magnetic cores from organic to aqueous, PEG-coated magnetic nanoparticles (MNPs-2) were obtained as DO-PEG absorbed on the inner hydrophobic oleic acid layer. In the PEGylated bilayer system, the hydrocarbons of both layers interdigitated through hydrophobic interactions and the outer PEG segment provided steric stabilization and water dispersibility to the superparamagnetic nanoparticles. When the bilayers were formed, it prevented particles aggregation relayed on hydrophobic interactions and steric repulsion. The mean hydrodynamic size, polydispersity index, and zeta potential of MNPs-2 (measured in distilled water) were 61.7 ± 1.5 nm, 0.31 ± 0.08, and –(6.03 ± 0.71) mV, respectively (mean ± SD, n = 3). TEM (Figure 5b) clearly showed the existence of individual particles and small clusters of particles. Magnetic cores were successfully encapsulated in the hydrophobic core of DO-PEG by self-assembly, and the particle size of PEG-coated magnetic nanoparticles was smaller than that of magnetic cores encapsulated in polymers (e.g., poly-DL-lactide-*co*-glycolide[22], polylactide[23]) typically used in developing other nanocarriers for drug delivery application. Otherwise, the self-assembly technique in transferring hydrophobic OA-coated magnetic cores from organic to aqueous was more efficient than complex conjugation chemistry by attaching polymer to the surface of iron oxide cores.

Structural analysis and magnetic measurements of MNPs

To characterize the products further, XRD pattern was carried out to identify the nanocrystalline structure. Figure 6a clearly indicated that the XRD pattern of MNPs-1 and MNPs-2 were similar to that of standard Fe_3O_4 structure, confirming the crystalline structure of the magnetite nanoparticles[32].

TGA was performed to confirm the coating formation and estimate the binding efficiency on the surface of MNPs. Figure 6b showed the weight loss result for MNPs-1 (25%) and MNPs-2 (93%). A slight weight loss was observed up to 250°C in both curves, probably because of the adsorbed water, while a significant weight loss was noticed between 250°C and 500°C. The weight loss for MNPs-1 was attributed to decomposition of oleic acid, corresponding to a monolayer of oleic acid on the surface, and the weight loss for MNP-2 was increased by 68%, mainly due to the decomposition of DO-PEG.

The nanoparticles were characterized by FTIR to confirm the absorbing of DO-PEG to the surface of the nanoparticles. FTIR spectra of OA-coated magnetic

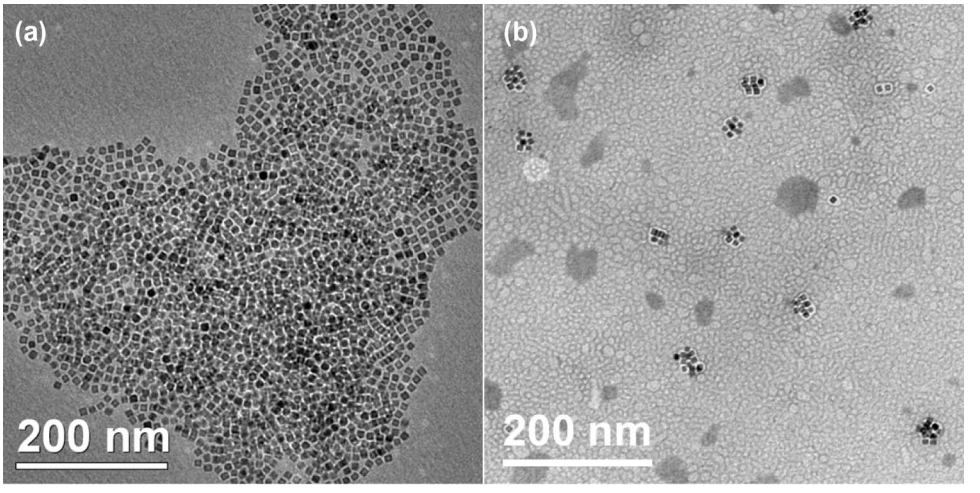

Figure 5. TEM images of (a) OA-coated magnetic nanoparticles (MNPs-1) dispersed in hexane and (b) PEG-coated magnetic nanoparticles (MNPs-2).

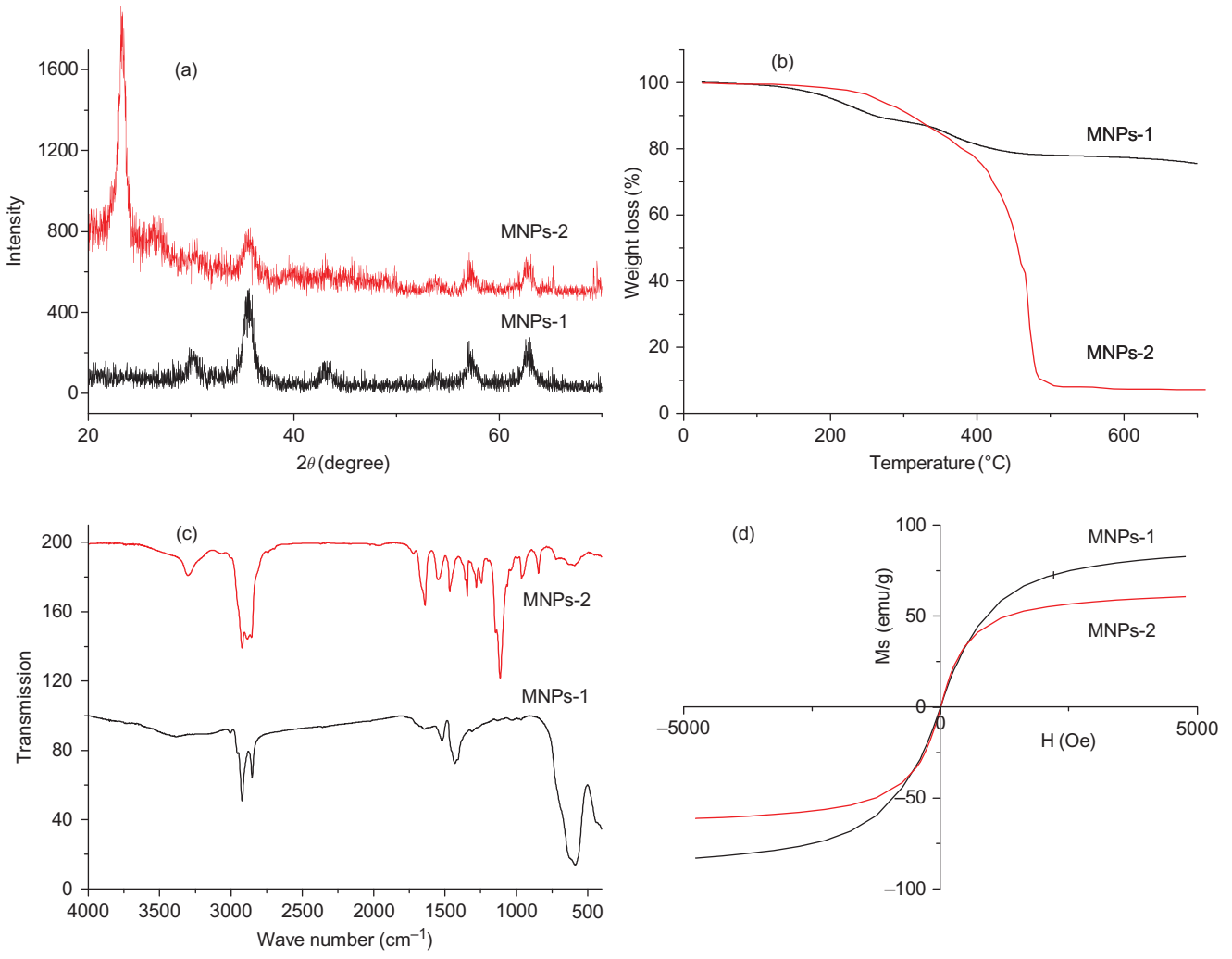

Figure 6. Characterization of the MNPs. (a) X-ray powder diffraction pattern of OA-coated magnetic nanoparticles (MNPs-1) and DO-PEG-coated magnetic nanoparticles (MNPs-2). (b) TGA curves of MNPs-1 and MNPs-2. (c) FT-IR spectra of MNPs-1 and MNPs-2. (d) Hysteresis loops at room temperature for MNPs-1 and MNPs-2.

nanoparticles and DO-PEG-coated nanoparticles were shown in Figure 6c. In spectrum of MNPs-1, the peaks at 1635 and 1526 cm^{-1} were attributed to the carboxylate (COO^-) unsymmetrical and symmetrical stretching vibration, respectively, indicating that oleic acid was bound to the surface of Fe_3O_4 nanoparticles through covalent bond between carboxylate (COO^-) and Fe atom[33]. The characteristic absorption bands of MNPs-1 at 590 cm^{-1} was attributed to Fe–O bonds. In the case of DO-PEG-coated Fe_3O_4 nanoparticles, the C–O–C ether stretch band at 1115 cm^{-1} and the vibration band at 1338 cm^{-1} (antisymmetric stretch) appeared in the FT-IR spectrum of the nanoparticles after surface modification. Similarly, the bands around 2916 and 959 cm^{-1} corresponded to –CH stretching vibrations and –CH out-of-plane bending vibrations, respectively. The C–O–C, –CH, and –CH peaks were strong evidence that DO-PEG was covered at the nanoparticle surface.

It was known that magnetic particles less than about 30 nm would exhibit superparamagnetism. Therefore, the prepared 10 nm MNPs had superparamagnetism. It was verified by the magnetization curve measured by VSM. A typical plot of magnetization versus applied magnetic field (M–H loop) was shown in Figure 6d. It provided evidence that both MNPs-1 and MNPs-2 were superparamagnetic at room temperature, with no hysteresis and perfect Langevin behavior[34]. MNPs-1 coated with DO-PEG maintained its crystalline structure. The saturation magnetization of the superparamagnetic nanoparticles coated with DO-PEG (60.7 ± 5.1 emu/g Fe, n=3) was lower than that of MNPs-1 (82.7 ± 4.6 emu/g Fe, n = 3). There were several approaches that could explain the reduction of saturation magnetization (Ms, emu/g, determined by VSM) for polymer-coated magnetic nanoparticles[35,36]. In this case, the presence of nonmagnetic surfactant molecules on the surface of

OA-coated magnetic nanoparticles led to decrease of the *Ms*, but the loss of magnetization during the encapsulation process was lower than that of large-sized microparticles (~40–50%) with limited encapsulation of iron oxide cores[24,37].

Stability analysis of PEG-coated magnetic nanoparticles at physiological conditions

To examine the stability of the MNPs under physiological conditions for use as MR contrast agents, we investigated the stability of MNPs in phosphate buffer saline (PBS) buffer solution, various pH and ionic strength conditions. The PEG-coated magnetic nanoparticles were fairy dispersed in PBS buffer solution as well as in the pH range from 3 to 10. As seen in Figure 7a, the hydrodynamic diameter of the particles varies between 55 and 65 nm as the pH changes, with no visible precipitation. Particles stability was also studied as a function of ionic strength at pH 7. The NaCl concentration was varied from 0.05 to 0.30 M, and as seen in Figure 7b, particles were stable in this range with no precipitation. To further verify the stability of the MNPs under physiological conditions, the size changes of particles upon incubation in cell culture medium containing 10% fetal bovine serum (FBS) as simulated in vivo plasma were monitored. As shown in Figure 7c, the hydrodynamic diameter of the particles was slightly altered by less than 5 nm after 24 hours of incubation in Roswell Park Memorial Institute (RPMI) medium containing 10% FBS. In addition, we could not observe any aggregates upon incubation in distilled water and PBS buffer solution (Figure 7c). This was mainly attributed to the antibiofouling property of the PEG coating layer that played a key role in not only preventing the particles from aggregation, which was a result of nonspecific protein or salt adsorption, but also providing good water dispersibility by exposing hydrophilic PEG layer on the surface of MNPs[15,16]. MNPs lacking the antibiofouling characteristic were easily taken up by reticuloendothelial system (RES). As the PEG-coated MNPs developed herein were fairly stable in a stimulated plasma solution without agglutination and besides maintained their size less than 100 nm, we postulated that the MNPs upon systemic circulation could be accumulated in tumor sites by EPR effect as a result of the presence of leaky vasculatures around tumors[9].

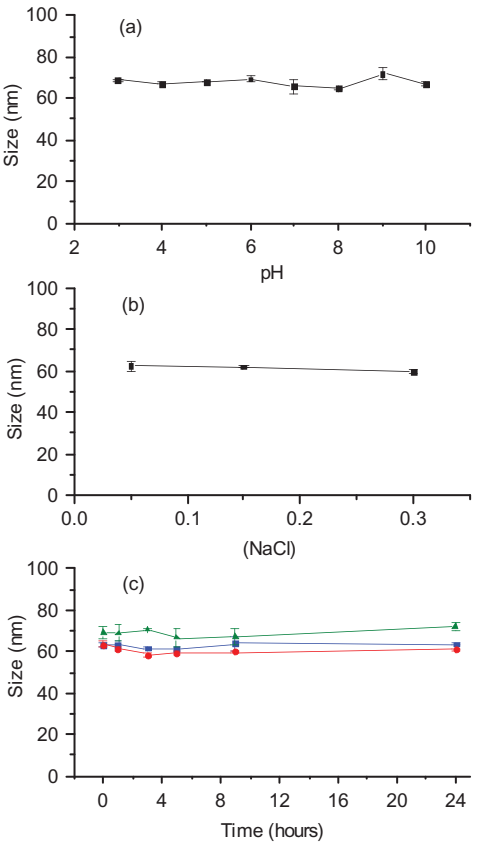

Figure 7. Stability of PEG-coated magnetic nanoparticles: (a) hydrodynamic diameter as a function of pH, (b) hydrodynamic diameter as a function of NaCl concentration at pH 7, (c) hydrodynamic diameter as a function time upon incubation in distilled water (■), PBS (●), and RPMI containing 10% FBS (▲).

MRI characteristics of MNPs

The T_2 relaxation process occurred because of the exchange of energy between protons in water molecules. In the presence of an externally applied magnetic field, inhomogeneity in the magnetic field was created by MNPs that resulted in dephasing of the magnetic moments of protons and hence T_2 shortening. The MRI signal intensity of MNPs decreased in varied degrees in T_2-weighted imaging depending on the Fe concentration in agarose solution. As the MNPs concentration, measured in μg Fe/mL, was increased in the agarose solution, the signal intensity decreased (Figure 8a and b). As the iron concentration increased from 0.004 to 0.800 μg Fe/mL, the T_2-relaxation times were reduced from 599.1 to 21.9 ms. The relaxation rate, $R_2 = 1/T_2$, was linearly proportional to the iron concentration (Figure 8c). T_2 relaxivity of our MNPs and Feridex IV[38] were 5.6 and 4.8 $s^{-1}\mu g^{-1}mL$, respectively. The relatively higher T_2 relaxivity of our MNPs relative to Feridex IV suggested a better contrast property of our MNPs and hence could be more sensitive as an MRI contrast agent. This was attributed to the ability of MNPs to induce more local inhomogeneity in the magnetic field than Feridex IV.

MRI is one of the present commonly used imaging technologies, which enables anatomical, functional, and even molecular information obtained noninvasively from intact organisms at high spatial resolution. MNPs are developed as contrast agents for MRI and

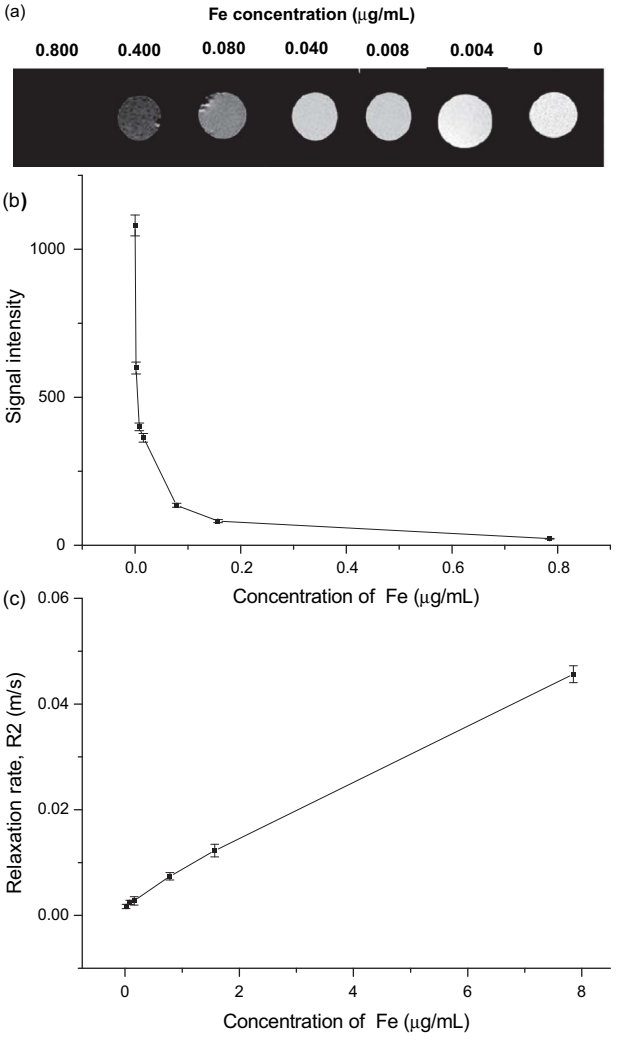

Figure 8. MRI properties of MNPs-2: (a) signal intensity-weighted images (TR = 2500 ms, TE = 10 ms) of MNPs in 2% agarose solution at various iron concentration at room temperature, blank agarose solution was taken as a control, (b) signal intensity of T_2 relaxation time at different iron concentration. (c) T_2 relaxation rate (R_2) of MNPs versus iron concentration.

increase the diagnostic sensitivity and specificity due to modifications of the relaxation time of the protons[39]. In this research, we formulated PEG-coated MNPs with desirable T_2 negative contrast effect in MRI. A key consideration for the in vivo use of MNPs for cancer imaging is lower uptake of particles by RES such as macrophages so that the MNPs can circulate long enough to be accumulated in the tumor by the EPR effect. Work on using these MNPs for bio-imaging, biodetection, and drug delivery is underway.

Conclusion

We have presented the fabrication of novel antifouling PEG-coated superparamagnetic iron oxide nanoparticles. The properties of iron oxide nanoparticles were determined by TEM, dynamic light scattering, XRD, TGA, FTIR, and VSM, respectively. The MNPs were highly stable in water at pH 3–10 and at salt concentration as high as 0.30 M NaCl. The stability of the MNPs in suspension is further confirmed by incubation with 10% FBS containing cell culture medium. The data show that the sizes of MNPs are not altered even after 24 hours, indicating a lack of protein adsorption on their surfaces. Additionally, the relatively higher T_2 relaxivity of MNPs relative to Feridex IV suggests a better MRI contrast property. These particles could potentially be used in a wide range of applications such as biotechnology, MRI, and magnetic fluid hyperthermia.

Acknowledgments

This work was partly supported by '211 project' and '985 project' university grant from Southeast University awarded to Dr. Xiong Fei (Nos. 4007031040 and 9207032444), National Basic Research Program of China (No. 2006CB933206), and National Natural Science Foundation of China (Nos. 60725101, 30870689, 30970754, and 20903021).

Declaration of interest

The authors report no conflicts of interest. The authors alone are responsible for the content and writing of this paper.

References

1. Tomita K, Tanimoto A, Irie R, Kikuchi M. (2008). Evaluating the severity of nonalcoholic steatohepatitis with superparamagnetic iron oxide-enhanced magnetic resonance imaging. J Magn Reson Imaging, 28:1444–50.
2. Gupta AK, Naregalkar RR, Vaidya VD, Gupta M. (2007). Nanoprobes and nanobiosensors for monitoring and imaging individual living cells. Nanomedicine, 2:22–30.
3. Jing XH, Yang K, Duan XJ, Xie B. (2008). In vivo MR imaging tracking of magnetic iron oxide nanoparticle labeled, engineered, autologous bone marrow mesenchymal stem cells following intra-articular injection. Joint Bone Spine, 75:432–8.
4. Sonvico F, Mornet S, Vasseur S, Dubernet C, Jaillard D. (2005). Folate-conjugated iron oxide nanoparticles for solid tumor targeting as potential specific magnetic hyperthermia mediators: Synthesis, physicochemical characterization, and in vitro experiments. Bioconjug Chem, 16:1181–8.
5. Talelli M, Rijcken CJ, Lammers T, Seevinck PR, Storm G. (2009). Superparamagnetic iron oxide nanoparticles encapsulated in biodegradable thermosensitive polymeric micelles: Toward a targeted nanomedicine suitable for image-guided drug delivery. Langmuir, 25:2060–7.
6. Horak D, Babic M, Jendelová P, Herynek V, Trchová M. (2007). D-mannose-modified iron oxide nanoparticles for stem cell labeling. Bioconjug Chem, 18:635–44.

7. Mahmoudi M, Simchi A, Milani AS, Stroeve P. (2009). Cell toxicity of superparamagnetic iron oxide nanoparticles. J Colloid Interface Sci, 336:510–8.
8. Aime S, Cabella C, Colombatto S, Crich SG, Ginolio E. (2002). Insights into the use of paramagnetic Gd(III) complexes in MR-molecular imaging investigations. J Magn Reson Imaging, 16:394–406.
9. Matsumura Y, Maeda H. (1986). A new concept for macromolecular therapeutics in cancer chemotherapy: Mechanism of tumoritropic accumulation of proteins and the antitumor agent smancs. Cancer Res, 46:6387–92.
10. Zhang HT, Ding J, Chow GM, Dong ZL. (2008). Engineering inorganic hybrid nanoparticles: Tuning combination fashions of gold, platinum, and iron oxide. Langmuir, 24:13197–202.
11. Teng X, Yang H. (2007). Iron oxide shell as the oxidation-resistant layer in $SmCo_5$@Fe_2O_3 core–shell magnetic nanoparticles. J Nanosci Nanotechnol, 7:356–61.
12. Shavel A, Liz-Marzán LM. (2009). Shape control of iron oxide nanoparticles. Phys Chem Chem Phys, 11:3762–6.
13. Park J, An K, Hwang Y. (2004). Ultra-large-scale syntheses of monodisperse nanocrystals. Nat Mater, 3:891–5.
14. Shi X, Thomas TP, Myc LA, Kotlyar A, Baker Jr JR. (2007). Synthesis, characterization, and intracellular uptake of carboxyl-terminated poly(amidoamine) dendrimer-stabilized iron oxide nanoparticles. Phys Chem Chem Phys, 9, 5712–20.
15. Pankhurst QA, Connolly J, Jones SK, Dobson J. (2003). Applications of magnetic nanoparticles in biomedicine. J Phys D Appl Phys, 36:R167–81.
16. Berry CC, Curtis ASG. (2003). Functionalisation of magnetic nanoparticles for applications in biomedicine. J Phys D Appl Phys, 36:R198–206.
17. Cui X, Antonietti M. (2006). Structural effects of iron oxide nanoparticles and iron ions on the hydrothermal carbonization of starch and rice carbohydrates. Small, 2:756–9.
18. Jarrett BR, Frendo M, Vogan J. (2007). Size-controlled synthesis of dextran sulfate coated iron oxide nanoparticles for magnetic resonance imaging. Nanotechnology, 18:35603–10.
19. Frankamp BL, Boal AK, Tuominen MT, Rotello VM. (2005). Direct control of the magnetic interaction between iron oxide nanoparticles through dendrimer-mediated self-assembly. J Am Chem Soc, 127:9731–5.
20. Larsen EK, Nielsen T, Wittenborn T, Birkedal H. (2009). Size-dependent accumulation of PEGylated silane-coated magnetic iron oxide nanoparticles in murine tumors. ACS Nano, 3:1947–51.
21. Narain R, Gonzales M, Hoffman AS, Stayton PS, Krishnan KM. (2007). Synthesis of monodisperse biotinylated p(NIPAAm)-coated iron oxide magnetic nanoparticles and their bioconjugation to streptavidin. Langmuir, 23:6299–304.
22. Okassa LN, Marchais H, Douziech-Eyrolles L. (2007). Optimization of iron oxide nanoparticles encapsulation within poly(d,l-lactide-co-glycolide) sub-micron particles. Eur J Pharm Biopharm, 67:31–8.
23. Arbab AS, Bashaw LA, Miller BR, Jordan EK. (2003). Characterization of biophysical and metabolic properties of cells labeled with superparamagnetic iron oxide nanoparticles and transfection agent for cellular MR imaging. Radiology, 229:838–46.
24. Strable E, Bulte JWM, Moskowitz B. (2001). Synthesis and characterization of soluble iron oxide-dendrimer. Chem Mater, 2001(13):2201–9.
25. Charvat TT, Lee DJ, Robinson WE. (2006). Design, synthesis, and biological evaluation of chicoric acid analogs as inhibitors of HIV-1 integrase. Bioorg Med Chem, 14:4552–67.
26. Xiong F, Li J, Wang H, Chen YJ. (2006). Synthesis, properties and application of a novel series of one-ended monooleate-modified poly(ethylene glycol) with active carboxylic terminal. Polymer, 47:6636–41.
27. Seguer J, Selve C, Allouch M, Infante M. (1996). Nonionic amphiphilic compounds from lysine as molecular mimics of lecithins. J Am Oil Chem Soc, 73:79–86.
28. Jana NR, Chen Y, Peng X. (2004). Size- and shape-controlled magnetic (Cr, Mn, Fe, Co, Ni) oxide nanocrystals via a simple and general approach. Chem Mater, 16:3931–5.
29. Mercadal M, Domingo JC, Petriz J, Garcia J. (2000). Preparation of immunoliposomes bearing poly(ethylene glycol)-coupled monoclonal antibody linked via a cleavable disulfide bond for ex vivo applications. Biochim Biophys Acta, 1509:299–310.
30. Hardy JG, Hirst AR, Ashworth I, Brennan C. (2007). Exploring molecular recognition pathways within a family of gelators with different hydrogen bonding motifs. Tetrahedron, 63:7397–406.
31. Ray GB, Chakraborty I, Moulik SP. (2006). Pyrene absorption can be a convenient method for probing critical micellar concentration (cmc) and indexing micellar polarity. J Colloid Interface Sci, 294:248–54.
32. Sun C, Sze R, Zhang M. (2006). Folic acid-PEG conjugated superparamagnetic nanoparticles for targeted cellular uptake and detection by MRI. J Biomed Mater Res B Appl Biomater, 78:550–7.
33. Ren YZ, Kato T. (2001). Structure of barium stearate films at the air/water interface investigated by polarization modulation infrared spectroscopy and π–A isotherms. Langmuir, 17:2688–93.
34. Chantrell RW, Popplewell J, Charles SW. (1978). Measurements of particle size distribution parameters in ferrofluids. IEEE Trans Magn, 14:975–7.
35. Popplewell J, Sakhinini L. (1995). The dependence of the physical and magnetic properties of magnetic fluids on particle size. J Magn Magn Mater, 149:72–8.
36. Mikhayaylvo M, Kim DK, Berry CC. (2004). BSA immobilization on amine-functionalized superparamagnetic iron oxide nanoparticles. Chem Mater, 16:2344–54.
37. Silva AK, Egito ES, Araujo IB. (2008). Development of superparamagnetic microparticles for biotechnological purposes. Drug Dev Ind Pharm, 34:1111–6.
38. Tapan KJ, Richey J, Strand M, Leslie-Pelecky DL. (2008). Magnetic nanoparticles with dual functional properties: Drug delivery and magnetic resonance imaging. Biomaterials, 29:4012–21.
39. Bordat C, Sich M, Rety F. (2000). Acoustic noise and functional magnetic resonance imaging: Current strategies and future prospects. J Magn Reson Imaging, 16:505–10.